



Global component analysis of errors in five satellite-only global precipitation estimates

Hanqing Chen^{a, b, c}, Bin Yong^{a, d}, Leyang Wang^c, Liliang Ren^{a, d}, Yang Hong^c

^a*State Key Laboratory of Hydrology-Water Resources and Hydraulic Engineering,*

5 *Hohai University, Nanjing 210098, China.*

^b*School of Earth Sciences and Engineering, Hohai University, Nanjing 211100, China.*

^c*Key Laboratory for Digital Land and Resources of Jiangxi Province, East China University of Technology, Nanchang 330013, China.*

^d*College of Hydrology and Water Resources, Hohai University, Nanjing 210098, China.*

10 ^e*School of Civil Engineering and Environment Sciences, University of Oklahoma, Norman, OK 73019, USA.*

Corresponding author: Bin Yong (yongbin@hhu.edu.cn)

Abstract: Revealing the error components for satellite-only precipitation products (SPPs) can help algorithm developers and end-users substantially understand their error features and meanwhile is fundamental to customize retrieval algorithms and error adjustment models. Two error decomposition schemes were employed to explore the error components for five SPPs (i.e., MERG-Late, IMERG-Early, GSMaP-MVK, GSMaP-NRT, and PERSIANN-CCS) over different seasons, rainfall intensities, and topography classes. Firstly, this study depicted global maps of the total bias (total mean squared error) and its three (two) independent components for these five SPPs over four seasons for the first time. We found that the evaluation results between similar regions could not be extended to one another. Hit and/or false biases are major components of

15
20



the total bias in most regions of the global land areas. In addition, the proportions of the systematic error are less than 20% of total errors in most areas. One should note that each SPP has larger systematic errors in several regions (i.e., Russia, China, and Conterminous United States) for all four seasons, these larger systematic errors from retrieval algorithms are primarily due to the missed precipitation. Furthermore, IMERG suite and GSMaP-NRT display less systematic error in the rain rates with intensity less than 40 mm/day, while the systematic errors of GSMaP-MVK and PERSIANN-CCS increase with increasing rainfall intensity. Given that mean elevation cannot reflect the complex degree of terrain, we introduced the standard deviation of elevation (SDE) to replace mean elevation to better describe topographic complexity. Compared with other SPPs, GSMaP suite shows a stronger topographic dependency in the four bias scores. A novel metric namely normalized error component (NEC) was proposed to fairly evaluate the impact of the solely topographic factor on systematic (random) error. It is found that these products show different topographic dependency patterns in systematic (random) error. Meanwhile, the pattern of the impact of the solely topographic factor on systematic (random) error is similar to the relationship between systematic (random) error and topography because the average precipitations of all topography categories are very close. Finally, the potential directions of the improvement in satellite precipitation retrieval algorithms and error adjustment models were identified in this study.

Keywords: Satellite precipitation; Error component; Systematic error; Rainfall intensity; Topography



45 1. Introduction

Precipitation is one of crucial inputs for hydrological cycle system and therefore obtaining the accurate precipitation data is of great significances for the study of global water cycle (Hou et al., 2014; Kidd et al., 2017; Chen et al., 2019a). Traditional methods depend on rain gauges to obtain the precise point-scale precipitation observations (Kidd
50 and Huffman, 2011b). In addition, ground-based radars can provide the accurate precipitation estimates over a range of approximately 250 km (Chen et al., 2019b). However, these two methods of measurement precipitation are affected by local environment, economy and other factors, and it is difficult to obtain the continuous spatiotemporal precipitation estimates over many regions of the world, especially over
55 complex mountainous and developing countries (Baez-Villanueva et al., 2020).

The satellite-based instruments have the ability to overcome the limitations of rain gauges and ground-based radars to provide the precipitation estimates with high spatiotemporal resolution and even covering the globe (Kidd et al., 2011a). However,
60 satellite precipitation products contain a large number of random errors, systematic errors and large uncertainties, especially over complex mountains (Tian et al., 2010a; Maggioni et al., 2016a; Chen et al., 2020). Therefore, it is necessary to comprehensively analyze the errors of satellite precipitation products, especially for their satellite-only versions. Over the past 20 years, there are many literatures to investigate the error
65 features of satellite precipitation products at global scale (e.g., Yong et al., 2015; Liu et al., 2016; Beck et al., 2017; Chen et al., 2020) and region scale (e.g., AghaKouchak et



al., 2011; Yong et al., 2010, 2013, 2016; Takido et al., 2016; Tan et al., 2017; Prakash
et al., 2018; Gebregiorgis et al., 2018; Beck et al., 2019; Chen et al., 2019b). These
studies provided a great deal of valuable information for algorithm developers and end-
70 users. However, most studies used relative bias/mean error to analyze the error features
of SPPs, which could be misleading due to the error average from different error
components. In some cases, relative bias/mean error is smaller even though the absolute
values of its error components are larger (Chen et al., 2019b).

75 Tian et al. (2009) proposed an error decomposition scheme to separate the total bias
into three independent components (i.e., hit bias, miss bias and false bias). This scheme
effectively avoided above-mentioned questions and is a fairer method to analyze errors.
To date there are several evaluation studies investigating major components of the total
bias for satellite precipitation products at several regions, such as mainland China (Yong
80 et al., 2016; Xu et al., 2016; Su et al., 2018; Chen et al., 2020), the contiguous United
States (Tian et al., 2009), central Asia (Guo et al., 2017). In terms of systematic error,
AghaKouchak et al. (2012) used an error decomposition technique proposed by
Willmott, (1981) to separate total mean squared error into systematic and random errors,
and analyzed systematic and random errors of the three satellite precipitation products
85 (i.e., CMORPH, PERSIANN, and real-time TMPA) over the entire conterminous
United States (COUNS). Maggioni et al. (2016b) further investigated the systematic
errors for TMPA products over COUNS. However, these studies were only concentrated
in limited regions and lacked the investigations at global scale. Meanwhile, the



transferability of the regional evaluation results to other similar areas still needs to be
90 investigated, which has always plagued algorithm developers and users. Besides, it
needs to figure out which component of total bias tends to produce larger systematic
errors.

Topography is a crucial factor that impacts the satellite precipitation retrievals (Tapiador
95 et al., 2012; Xu et al., 2017; Chen et al., 2019b). Several studies strive to investigate the
total bias of satellite precipitation retrievals under different terrains (e.g., Takido et al.,
2016; Guo et al., 2017; Xu et al., 2017; Chen et al., 2019b). Nevertheless, the analysis
of error components for satellite precipitation estimates under different topography
categories is lacking in previous studies. In particular, there is no literature to investigate
100 the potential link between systematic (random) error and terrain. Meanwhile, the impact
of the solely topographic factor on systematic and random errors is not clear due to
lacking relevant investigations in previous studies. These limitations inherent in
previous studies block the characterization of satellite precipitation error. Furthermore,
previous literatures used mean elevation to describe the terrain of the grid cell, yet the
105 mean elevation of each pixel often cannot objectively represent the complexity of the
topography. A more reasonable metric is needed to be introduced to describe the
topography of the grid cell.

Precipitation intensity is also an important factor associated with the errors of satellite
110 precipitation estimates (Chen et al., 2020). Previous efforts found that satellite



precipitation products overestimated the precipitation in the light rainfall events and underestimated the precipitation in the heavy rainfall events (Tian et al., 2009; Kirstetter et al., 2013; Chen et al., 2013). Tian et al. (2009) investigated the major components of the total bias for different rainfall intensities, and Maggioni et al. (2016b) revealed the
115 relationship between the systematic (random) error and rainfall intensity for TMPA products. Nevertheless, the potential link between the systematic (random) error components of five evaluated SPPs and precipitation intensity is still absent.

Consequently, the objectives of this study include five-fold: (1) to investigate the major
120 components of errors (including total bias and total mean squared error) for five SPPs including IMERG Late run (IMERG-Late), IMERG Early run (IMERG-Early), GSMaP Microwave-IR Combined Product (GSMaP-MVK), GSMaP in Near-Real-Time (GSMaP-NRT), and PERSIANN Cloud Classification System (PERSIANN-CCS) for four seasons across global land areas; (2) to investigate the potential for the
125 transferability of the regional assessment results to other similar regions; (3) to analyze the major components of the total bias and total mean squared error for five SPPs under different rainfall intensities; (4) to analyze the major components of the total error for five SPPs under different terrains and study the impact of the solely topographic factor on systematic and random errors; (5) to answer the question which component of the
130 total bias tends to produce larger systematic errors.



2. Study area, datasets and methodology

2.1 Study area

Our study areas cover the global land areas (60°N/S). Fig.1a shows the topographic relief across the global land areas, the standard deviation of elevation (SDE) (more
135 information on this concept see methodology section) was introduced to better describe the terrain of the grid cell. The complex degree of the topography increases with increasing color depth, the areas with a rather complex terrain mainly include western COUNS, Andean mountains, southern Europe, Turkey, Iran, Afghanistan, Tibetan Plateau (TP), most humid regions in mainland China, Japan, and so on. Furthermore,
140 the global land areas can be divided into four climate regions namely humid regions (average annual precipitation (AAP) > 800mm/yr), semi-humid regions (AAP between 400 – 800 mm/yr), semi-arid regions (AAP between 200 – 400 mm/yr), and arid regions (AAP < 200 mm/yr) (see Fig. 1b). The detail information about the climate region can be found in Fig.1c.

145 2.2 Datasets

2.1.1 Reference products

To achieve the objectives of this study, three high-accuracy rain gauge data sets are employed as the references. Climate Precipitation Center unified (CPCU) data was used as the benchmark over the global land areas except for mainland China. CPCU produces
150 continuous daily precipitation at 0.5° spatial resolution using optimal interpolation (OI) based on > 17,000 gauges (Xie et al., 2007; Chen et al., 2008). For the benchmark over



mainland China, China Gauge-based Daily Precipitation Analysis (CGDPA) data was employed as one of the references. This dataset, with 0.25° spatial and daily temporal resolution, was developed from ~ 2400 rain gauges, using OI method. The assessment results indicated that this ground-based precipitation dataset outperforms CPCU data and East Asia gauge analysis (EA_Gauge; Xie et al., 2007) over mainland China (Shen and Xiong, 2016). Regarding the component analysis of errors for five SPPs in different topographies, high-accuracy and high spatiotemporal resolution (hourly temporal and 0.1° spatial resolution) ground observations from 26326 rain gauges were used as the benchmark. The spatial distribution of the rain gauge can be found in our published paper (i.e., Chen et al., 2019b; Chen et al., 2020). However, this product has large uncertainties in cold seasons due to freezing weather. The analysis is executed at a finer spatial resolution (0.1°), which avoids the smoothing of topography relief as much as possible. In this study, only the pixels with at least one rain gauge are considered, the spatial distribution of rain gauges (including CPCU and CGDPA) is shown in Fig. 1d.

2.1.2 Satellite-only precipitation products

The main focus of this study is to analyze the components of error for five SPPs including IMERG-Late V6, IMERG-Early V6, GSMaP-MVK V7, GSMaP-NRT V6/V7, PERSIANN-CCS over global land areas. Given that the gauge-adjusted satellite precipitation products (e.g., IMERG Final run, gauge-adjusted GSMaP, and PERSIANN Climate Data Record) merge the ground-based rain gauge observations, these gauge-adjusted products did not employ in this study. It is because the overlaps between gauge-adjusted products and benchmark result in some potential evaluation



uncertainties, especially for gauge-adjusted GSMaP that fuses CPCU data. Additionally,
175 purely satellite-derived version of CMORPH and real-time TMPA are excluded because
the long-term satellite-only version of CMORPH was no longer released to the public
and the real-time TMPA had stopped update on December 31, 2019
(<https://gpm.nasa.gov/>). Finally, the 5-year (2015-2019) period data of these five SPPs
is chosen to investigate their error components across global land areas. The detailed
180 information about the production processes of these five SPPs can be found in our
previous paper (i.e., Chen et al., 2020).

In global analysis, all SPPs need to be resampled to the 0.5° spatial resolution and
aggregated to daily temporal resolution. This is for consistency with CPCU data (0.5°,
185 daily). The information of these five SPPs is listed in Table 1.

2.3 Methodology

2.3.1 Error decomposition technique

Tian et al. (2009) proposed an error decomposition scheme to separate the total bias
(TB) into hit bias (HB), miss bias (MB), and false bias (FB). This technique is more
190 effective in identifying the major error components of the total bias, which can provide
valuable information to customize retrieval algorithms and remove errors. The four bias
scores can be defined as follows (Tian et al., 2009):

$$TB = \frac{\sum(S-G)}{\sum G} \times 100\% \quad (1)$$

$$HB = \frac{\sum(S_H - G_H)}{\sum G} \times 100\% \quad (2)$$

$$195 \quad MB = \frac{-\sum G_M}{\sum G} \times 100\% \quad (3)$$



$$FB = \frac{\sum S_F}{\sum G} \times 100\% \quad (4)$$

$$TB = HB + MB + FB \quad (5)$$

where S and G are the precipitation measured by satellite and rain gauge, respectively; S_H and G_H are the precipitation estimates of hit events for satellite and rain gauge, respectively; G_M denotes the precipitation missed by satellite in miss rainfall events; S_F indicates the precipitation measured by satellite in false rainfall events.

Another error decomposition technique is to decompose the total mean squared error into systematic and random error components. This strategy was used to separate numerical weather prediction models into systematic and random errors by Willmott, (1981). Subsequently, AghaKouchark et al. (2012) employed this technique to investigate the systematic and random errors of the three satellite precipitation products (i.e., CMORPH, PERSIANN, and real-time TMPA) over CONUS. This error decomposition method can be defined as follows (Willmott, 1981; AghaKouchark et al., 2012):

$$\frac{1}{n}(\sum_{i=1}^n (S - G)^2) = \frac{1}{n}(\sum_{i=1}^n (\hat{S} - G)^2) + \frac{1}{n}(\sum_{i=1}^n (S - \hat{S})^2) \quad (6)$$

$$E_S = 100\% \times (\sum_{i=1}^n (\hat{S} - G)^2) / (\sum_{i=1}^n (S - G)^2) \quad (7)$$

$$E_R = 100\% \times (\sum_{i=1}^n (S - \hat{S})^2) / (\sum_{i=1}^n (S - G)^2) \quad (8)$$

$$\hat{S} = a \times G + b \quad (9)$$

where E_S and E_R represent the systematic and random components of error, respectively; a and b are slope and intercept, respectively, and they can be computed by using least square method. Note that the systematic error component (E_S) plus



random error component (E_R) is 100%.

220 2.3.2 Normalized error component

The systematic and random errors of SPPs are impacted by several crucial factors, such as season and rainfall intensity (AghaKouchark et al., 2012; Maggioni et al., 2016b).

The differences in precipitation intensity may be inevitable between various topographies, which hinders the study of influence of the solely topographic factor on systematic (random) error. Thus, a novel metric called normalized error component (NEC) was proposed to strictly explore the impact of the solely topographic factor on systematic and random errors. This metric can be defined as follows:

$$NEC = \left(\sum_{i=1}^n (\hat{S} - G)^2 \right) / \left(\left(\sum_{i=1}^n (S - G)^2 \right) \times \bar{G} \right) \quad (10)$$

where \bar{G} indicates the mean value of ground-based observations.

230 2.3.3 Index of topography complexity

Mean elevation cannot reflect the complex degree of the terrain, using the errors of SPPs as a function of the mean elevation to study the relationship between errors and topography is unreasonable. To better describe the complex degree of the topography for each grid cell, we proposed standard deviation of elevation (SDE) instead of average elevation to describe topographic complexity. This score effectively reflects the topography relief. The larger the SDE value, the greater the relief of topography. The calculated formula of SDE can be defined as follows:

$$\begin{cases} \bar{E} = \frac{1}{n} \sum E_i \\ SDE = \sqrt{\frac{1}{n} \sum (E_i - \bar{E})^2} \end{cases} \quad (11)$$

where \bar{E} indicates the mean value of elevation for each pixel; E_i denotes i th elevation



240 value of each grid cell; n represents sample size of each pixel. The SDE values of the
global land areas are shown in Fig. 1a. The error and its components as a function of
SDE are used to analyze the major error components for five evaluated SPPs under
different topographies. Similarly, the relationship between error/its components and
precipitation intensity is established for revealing the major error components of SPPs
245 in different rainfall intensities.

3. Results

3.1 Global view of error components

3.1.1 Spatial analysis of error components for the total bias over different seasons

This is known to all that the errors of SPPs have a strongly seasonal dependency, and
250 the analysis associated with the total bias and its major error components is therefore
necessary to perform from different seasons. We implemented the following seasonal
division scheme: (1) spring (Mar – May, hereafter refer to as MAM); (2) summer (Jun
– Aug, hereafter refer to as JJA); (3) autumn (Sep – Nov, hereafter refer to as SON); (4)
winter (Dec – Feb, hereafter refer to as DJF). Note that the results of IMERG-Early and
255 GSMaP-NRT are almost the same with those of IMERG-Late and GSMaP-MVK,
respectively. It is attributed to a tiny difference in their algorithms used. Consequently,
the global maps of the four bias scores (i.e., total bias, hit bias, miss bias, and false bias)
and the systematic error for IMERG-Early and GSMaP-NRT for four seasons are shown
in the supplementary materials (see Figs.S1 – S5).

260



For MAM season (Figs.2 and S1), the majority of SPPs share considerable similarities in total bias. IMERG suite (i.e., IMERG-Early and IMERG-Late) and GSMaP suite (i.e., GSMaP-NRT and GSMaP-MVK) seriously overestimated the precipitation (total bias > 100%) over most regions of the globe, such as the humid regions of COUNS, Mexico, Europe, India, and the semi-humid areas of China (see Figs. 2a, e). Yet, the total bias from different areas came from different error components. The total biases of the two suites are mainly dominated by hit component in COUNS and Europe, while the hit and false errors are major error components in Mexico and India. Additionally, total bias was dominated by false errors in China, however, missed precipitation is another major component for these two suites. As for PERSIANN-CCS, its larger total biases were primarily appearing in COUNS (except for its humid regions), Mexico, Brazil, and most of land areas in Asia (except for humid regions in China). Correspondingly, these larger total biases came from hit and false components over COUNS and Brazil, while they were dominated by false errors over Asia and Mexico.

275

Of JJA season (Figs. 3 and S2), over most areas of COUNS, five SPPs exhibit large overestimations (total bias > 80%), which primarily owes to the hit error component for IMERG suite and GSMaP suite. As for Mexico, the precipitation is evidently overestimated by these five SPPs in northwest, and the main error components are hit bias. Regarding Europe, the hit error component is the major error components for IMERG suite and GSMaP suite. However, PERSIANN-CCS underestimated precipitation over most regions of Europe. That is due to miss errors and hit errors. In

280



addition, a majority of evaluated SPPs show relatively better performance in mainland
China during JJA season (summer), with lower total bias of $\pm 20\%$. However, it cannot
285 be ignored that miss and false biases for these SPPs are relatively larger over mainland
China despite these two error components canceling one another.

For SON season (Figs. 4 and S3), SPPs share considerable differences in the error
features. Over COUNS, IMERG suite displays relatively low overestimations and
290 underestimations over most regions. However, GSMaP suite seriously overestimated
the precipitation due to its larger hit biases. For PERSIANN-CCS, it evidently
overestimated the precipitation in arid and semi-arid regions, which is attributed to hit
and false components. Conversely, obviously underestimation precipitation is over
southeastern regions, and the hit error is major error components. Over China, IMERG
295 suite shows slight underestimations or overestimations over most regions although miss
bias and false bias are relatively larger, this feature is similar to that in JJA season. For
GSMaP suite and PERSIANN-CCS, they sorely underestimated (overestimated)
precipitation in humid areas (the residual regions of China) due to larger missed
precipitation (false error component). On the other hand, all SPPs have a common
300 feature that their total biases are very similar to their respective hit component over
Mexico, Brazil, Europe, and India because of missed precipitation and false bias
canceling one another.

Global maps of the four bias metrics for five SPPs over DJF season are shown in Figs.



305 5 and S4. One can be seen that five SPPs show an obvious similarity in error characteristics in Brazil and Australia, their total biases are very similar to their respective hit components. On the other hand, the differences in spatial maps of the four bias scores primarily exist in COUNS, Europe, and China. The discrepancies of retrieval algorithms and input sources used in these satellite product systems lead to
310 these differences.

Finally, the summary of the total bias and its major error components for these SPPs in main regions of the world is listed in supplementary materials to help readers quickly finding the needed information, see Table S1.

315 **3.1.2 Spatial analysis of the systematic error over different seasons**

These five SPPs share considerable similarities in the global maps of systematic errors in most areas of the global land areas for four seasons, with the systematic error of less than 20% of total mean squared error, as shown in Figs. 6 and S5. It means that the random error is the leading error component of the total mean squared error in most
320 regions of the global land areas. Also, these SPPs show an evidently seasonal dependency in several regions, such as COUNS, China, and Russia. IMERG suite has relatively larger systematic errors of exceeding 80% in the semi-humid and semi-arid regions of COUNS during DJF season. Similarly, the systematic errors of IMERG suite are very large for DJF season in mainland China except for humid regions and the
325 proportions are over 90%. For GSMaP suite, the seasonal feature mainly occurs in mainland China and Russia. It can be seen that there are larger systematic errors in DJF



season than other seasons over Russia. Meanwhile, it cannot be ignored that GSMaP suite exhibits large proportions of the systematic error for SON season in most humid regions of China. Finally, the proportions of the systematic error for PERSIANN-CCS
330 have an obvious feature of seasonality dependency in China, Europe, and eastern COUNS and are relatively larger in the parts of these areas, especially over China.

3.2 Error components of different precipitation intensities

The three bias scores (i.e., total bias, hit bias, and false bias) of five SPPs in different rainfall intensities are shown in Fig. 7. Note that false error component does not exist
335 because rainfall intensity categories are from the benchmark. Generally speaking, these SPPs show a high degree of consistency in three bias scores in different precipitation intensities. In addition, hit bias is the major error component in most rainfall intensities. Compared with other SPPs, GSMaP-NRT shows relatively larger biases in the light rainfall events (1-2 mm/day). It can be due to lacking backward-propagated PMW in
340 morphing process, which leads to seriously overestimate the precipitation values in the light rainfall events.

On the other hand, the variations of the systematic error for these five SPPs with six rainfall intensities are depicted in Fig. 8. Each SPP shows unique variations of
345 systematic errors with increasing precipitation intensities. One can be seen that IMERG suite and GSMaP-NRT have less systematic error (close to 0%) in the rainfall events less than 40mm/day. In contrast, the proportions of the systematic error for residual SPPs (i.e., GSMaP-MVK and PERSIANN-CCS) increase with increasing rainfall



intensity, indicating that the proportions of the systematic error for the two SPPs are
350 strongly related to precipitation intensity. Additionally, all SPPs have relatively larger
proportions of the systematic error when rainfall intensity is over 40mm/day. Besides,
all SPPs underestimated the precipitation volume in the heavy rainfall events with
intensity exceeding 40mm/day (see Fig. 7). The underestimated precipitation of these
SPPs in such heavy rainfall events might result in generating large systematic errors.

355 **3.3 Error components of different topographies**

In this section, the analysis is executed at finer spatiotemporal resolution (0.1°, hourly)
so as to avoid the smoothing of topography relief. Additionally, in order to exclude the
interferences of other factors (e.g., climate region and season) on conclusions, the
humid regions of China for JJA (summer) season are chosen to explore the major
360 components of the total bias and total mean squared error under different topography
categories.

The four bias metrics of five SPPs for different terrains are shown in Fig. 9. These
evaluated SPPs share some similarities in the variations of the four bias scores with
365 terrain. One of the common features is that their miss biases increase with increasing
terrain. Another is that the underestimated (overestimated) precipitation mainly came
from miss (false) bias. The performance of all evaluated SPPs is impacted by
topography in different extents. Relatively, the four biases metrics of GSMaP suite
display significantly topographic dependency, especially for false and hit error
370 components. This may be because the orographic/non-orographic rainfall classification



scheme used in the GSMaP retrieval system tends to overestimate the precipitation in the hit orographic rainfall events and capture the false-positive of the orographic rainfall (Yamamoto and Shige, 2015).

375 Fig. 10a shows the proportions of the systematic error for five SPPs under eleven terrain categories. Obviously, the systematic errors of all SPPs have a strongly topographic dependency, however, different SPPs exhibit distinct dependency patterns of topography. The proportions of the systematic error for IMERG suite increase with increasing topography complexity. While GSMaP suite and PERSIANN-CCS share a
380 common feature that their proportions of the systematic error increase with increasing topography complexity when SDE values are below 300 m and they decrease starting from 300 m. Compared with other evaluated SPPs, PERSIANN-CCS has relatively larger systematic errors in all topography categories. Nevertheless, these results shown in Fig. 10a may be impacted by rainfall intensity. Therefore, the influence of the solely
385 topographic factor on the systematic error is still unclear. This issue is substantially investigated in discussion section, see section 4.2.

4. Discussion

4.1 Potential for the transferability of the regional assessment results to other areas

390 There are many evaluation results associated with mainstream SPPs over most regions of the earth's land, such as COUNS, Europe, India, China, and so on. On the other hand, these SPPs lack necessary assessment in many regions with sparse ground observations,



such as Africa, central Australia, Mongolia, and so on. Using available evaluation results extended to other similar areas is an effective method that understands the performance of satellite precipitation products in the areas with sparse ground observations. Consequently, whether the evaluation results between similar regions can be extended to one another is a scientific question that needs to be answered urgently.

The comparisons in errors between the humid regions of COUNS and China are regarded as a representative example for analysis because these two chosen areas are located in the same latitude and have similar AAP (see Figs. 1b, c). In addition, these two selected areas are dominated by monsoon climate. One can see that all evaluated SPPs exhibit relatively larger discrepancies in spatial maps of the four bias scores for all four seasons over these two selected study areas (see Figs. 2-5). Similarly, these two chosen humid areas also have larger differences in the spatial maps of the systematic error (see Fig. 6). In addition, there are no any two areas where the assessment results can be extended to one another in the residual land areas of the world. Our previous study (i.e., Chen et al., 2019b) found that the large performance differences exist between various sensors. Meanwhile, the sensors onboard different satellites exist significant differences in the spatial maps of the sampling frequency (see Fig. 2 in Chen et al., 2019b). These analysis results further indicated that the evaluation results of SPPs from different areas might be large discrepancy due to the differences of the satellite samples used in satellite precipitation retrieval systems between various areas. Therefore, it can be concluded that the evaluation results between similar areas could



415 not be extended to one another. Future evaluation efforts should be focused on the
ungauged regions and the exploration of the novel evaluation methods that do not
depend on ground observations.

4.2 Impact of topography on the systematic error

In section 3.2, the results indicated that systematic errors are related to rainfall intensity
420 to some extent. Although we used the humid regions of China as study areas and
analyzed in summer season to alleviate the interferences of the climate and season
factors on the systematic error for these five SPPs. However, the discrepancies in
precipitation intensity are inevitable between different topography categories, which
affect the proportions of the systematic error for these products. Thus, we proposed
425 NEC metric to exclude the impact of the precipitation intensity on systematic error and
subsequently assessed the influence of the solely topographic factor on systematic error.

Fig. 10b shows the variations of NEC values for five evaluated SPPs by SDE for
summer season over the humid regions of China. It is obvious that the relationship
430 between the NEC and SDE is highly similar to the relationship between systematic error
and SDE. We found that the fundamental reason in the similarity of the two
relationships is that the mean precipitations (i.e., \bar{G} , see equation (10)) of all SDEs are
very close, with around 0.24 mm/h. According to the results shown in Fig. 10b, the
impacts of the topography on the proportions of the systematic error for IMERG suite
435 increase with increasing terrain complexity. For GSMaP suite and PERSIANN-CCS,
their proportions of the systematic error are positive correlation with topographic



complexity when the SDE value is less than 300 m. However, they are negative correlation starting from 300 m.

4.3 Which component of the total bias tends to produce larger systematic error?

440 Speaking generally, the proportions of the systematic error for five evaluated SPPs are below 20% for all four seasons over most areas of the global land areas. However, it cannot be ignored that these SPPs have larger systematic errors in several regions, such as parts of COUNS, China and Russia (see Fig. 6). In addition, we found that these areas with larger systematic errors always have relatively larger miss biases (see Figs. 445 2-6). Thus, there is a very attractive question whether miss bias tends to produce larger systematic errors. According to the definition of systematic and random errors (see equations (7-8)), missed precipitation tends to produce larger systematic error relative to hit and false biases. We believe that missed precipitation is a definitive factor producing larger systematic errors.

450 4.4 Potential directions of the improvement in satellite retrieval algorithms and error adjustment models

According to the results shown in this study, all evaluated SPPs have larger errors over most areas of the global land areas, suggesting that the quality of these evaluated SPPs have larger room for further improvement.

455

First, currently several studies attempted to reduce the errors of satellite-derived precipitation retrievals only considering seasonal and/or topographic factors into their error adjustment models or blending algorithms (e.g., Tian et al., 2010b; Hashemi et al.,



2017; Bhuiyan et al., 2018; Le et al., 2018; Choubin et al., 2019; Shen et al., 2019;
460 Baez-Villanueva et al., 2020). In practice, we found that the errors of these five
evaluated SPPs show significantly regional features. Meanwhile, the impact of several
crucial factors (i.e., topography, season, climate, and rainfall intensity) on the errors of
satellite precipitation estimates is very remarkable and has been proved in the results of
this study and our previous studies (i.e., Chen et al., 2019b, 2020). Consequently, there
465 are reasons to believe that incorporating all four factors (i.e., topography, season,
climate region/different areas, and rainfall intensity) into error adjustment models and
blending algorithms is expected to further reduce the errors of satellite precipitation
estimates.

470 Second, the global maps of the total bias (and total mean squared error) and its three
(and two) components for five evaluated SPPs were given in this paper. The results
indicated that the hit and/or false errors are the major error components of the total bias
for these SPPs over most regions of global land areas except for China, while the total
biases of these SPPs primarily came from miss and false biases in China. In addition,
475 the random error is the major component of the total mean squared error for these
evaluated SPPs in most regions of the global land areas. Consequently, the satellite
retrieval algorithms and error adjustment algorithms should focus on the reduction of
hit and false biases inherent in these SPPs over most regions of the world. For China,
the target of the improvement in future retrieval algorithms is to reduce miss and false
480 biases for these five SPPs.



Finally, the results of this paper are useful to improvement the adjustment algorithms for gauge-adjusted version of GSMaP (GSMaP-Gauge) because this gauge-adjusted product was made of GSMaP-MVK adjusted by CPCU data.

485 5. Conclusion

This paper executed the investigations on the major error components of the total error (including total bias and total mean squared error) for five SPPs (i.e., IMERG-Early, IMERG-Late, GSMaP-NRT, GSMaP-MVK, and PERSIANN-CCS) over different seasons, rainfall intensities, and terrains. The major conclusions based on the study
490 results are summarized as follows:

1. This paper is the first to depict the global maps of the total bias (total mean squared error) and its three (two) independent components for five SPPs over four seasons. We found that these five SPPs have remarkably regional features in error, and the evaluation results between similar regions could not be copied
495 to one another. This is due to the differences of satellite samples used in satellite precipitation retrieval systems between different areas. On the other hand, this finding indicated that the assessment of satellite precipitation products is very necessary over various regions of the world. Future efforts should focus on the areas still lacking evaluation and investigating novel
500 evaluation techniques that do not rely on ground-based observations.
2. Hit and/or false errors are the major components of the total bias for five SPPs evaluated over most areas of the world except for China (see Table S1), while



miss and false biases are the two major error components in China in spite of partially mutual cancellations between these two components. In terms of the systematic error, the proportions of the systematic error for these five evaluated

505

SPPs are below 20% over most areas of the global land areas. Nevertheless, they have an evident feature of seasonality dependency in several regions, such as COUNS, China, and Russia. Besides, we found that the areas with larger proportions of the systematic error always have larger missed precipitation.

510

According to equations (7-8), the large miss bias leads to generate larger systematic error. Thus, it can be concluded that missed precipitation is a decisive factor producing larger systematic errors.

3. All SPPs except for GSMaP-NRT exhibit a high degree of consistency in the three bias scores (i.e., total bias, hit bias, and miss bias) under different rainfall

515

intensities, their total biases primarily came from the hit component. On the contrary, each SPP has its own characteristics in the relationship between the systematic error and precipitation intensity. Besides, we found that all SPPs have relatively larger proportions of the systematic error in the rainfall events with intensity exceeding 40 mm/day.

520

4. We introduced standard deviation of elevation to replace mean elevation to better depict the topographic situations of the grid cell. Overall, all SPPs share considerable similarities in the four bias metrics (i.e., total bias, hit bias, miss bias, and false bias) under most terrain classes. Relatively, the four bias scores of GSMaP suite have a stronger topographic dependency, especially for false



525 bias and hit bias. The main cause may be that the orographic rainfall retrieval
module used in GSMaP retrieval system tends to overestimate the precipitation
in the hit orographic rainfall events and capture the false-positive of the
orographic rainfall. Furthermore, we found that these five SPPs exhibit
distinctly various topographic dependency patterns in systematic error. A novel
530 metric namely normalized error component was proposed to strictly evaluate
the influence of the solely topographic factor on systematic error. It is found
that the pattern of the impact of the solely topographic factor on systematic
errors is almost the same with the relationship between systematic error and
topography, primarily due to mean precipitation (i.e., \bar{G} , see equation (10)) of
535 around 0.24 mm/h in all terrain categories.

We hope that the new findings reported in this paper will be useful to improvement of
satellite precipitation retrieval algorithms and error adjustment models and to
improvement the potential applications of these products.

Author contribution statement

540 **Hanqing Chen:** Conceptualization, Methodology, Software, Formal analysis, Writing,
Funding Acquisition. **Bin Yong:** Writing – Review & editing, Project Administration,
Funding Acquisition. **Leyang Wang:** Writing – Review & editing, Methodology.
Liliang Ren: Conceptualization. **Yang Hong:** Conceptualization.

Competing interests

545 The authors declare that they have no conflict of interest.



Acknowledgments

We would like to express our most sincere thanks to the satellite precipitation products developers and ground-based precipitation products providers. The IMERG suite data can be obtained from <https://pmm.nasa.gov/data-access/downloads/gpm>; the
550 GSMaP suite data are obtained from <ftp://rainmap:Niskur+1404@hokusai.eorc.jaxa.jp/>;
the ground-based data in mainland China can be downloaded from <http://data.cma.cn>;
the CPCU data can be downloaded from <ftp://ftp.cpc.ncep.noaa.gov/precip/>. This work
was supported by National Key Research and Development Program of China (No. 2018YFA0605402) and National Natural Science Foundation of China (No. 51979073).
555 In addition, this work is partially supported by Key Laboratory for Digital Land and
Resources of Jiangxi Province, East China University of Technology (No. DLLJ201907).

References

- AghaKouchak, A., Behrangi, A., Sorooshian, S., Hsu, K., and Amitai, E.: Evaluation of
560 satellite retrieved extreme precipitation rates across the central United States, *J. Geophys. Res.-Atmos.*, 116, <https://doi.org/10.1029/2010JD014741>, 2011.
- AghaKouchak, A., Mehran, A., Norouzi, H., and Behrangi, A.: Systematic and random error components in satellite precipitation data sets, *Geophys. Res. Lett.*, 39, <https://doi.org/10.1029/2012GL051592>, 2012.
- 565 Baez-Villanueva, O. M., Zambrano-Bigiarini, M., Beck, H. E., McNamara, I., Ribbe, L., Nauditt, A., Birkel, C., Verbist, K., Giraldo-Osorio, J. D., and Thinh, N. X.: RF-



- MEP: A novel random forest method for merging gridded precipitation products and ground-based measurements, *Remote Sens. Environ.*, 239: 111606, <https://doi.org/10.1016/j.rse.2019.111606>, 2020.
- 570 Beck, H. E., Pan, M., Roy, T., Weedon, G. P., Pappenberger, F., van Dijk, A. I., Huffman, G. J., Adler, R. F., and Wood, E. F.: Daily evaluation of 26 precipitation datasets using Stage-IV gauge-radar data for the CONUS, *Hydrol. Earth Syst. Sci.*, 23(1), 207-224, 2019.
- Beck, H. E., Vergopolan, N., Pan, M., Levizzani, V., van Dijk, A. I., Weedon, G. P.,
575 Brocca, L., Pappenberger, F., Huffman, G. J., and Wood, E. F.: Global-scale evaluation of 22 precipitation datasets using gauge observations and hydrological modeling, *Hydrol. Earth Syst. Sci.*, 21(12), 6201-6217, 2017.
- Bhuiyan, A. E., Nikolopoulos, E. I., Anagnostou, E. N., Quintanasegui, P., and Barellaortiz, A.: A nonparametric statistical technique for combining global
580 precipitation datasets: development and hydrological evaluation over the Iberian Peninsula, *Hydrol. Earth Syst. Sci.*, 22(2), 1-28, 2017.
- Chen, H., Lu, D., Zhou, Z., Zhu, Z., Ren, Y., and Yong B.: An overview of the evaluation of satellite precipitation Products for Global Precipitation Measurement (GPM) (in Chinese), *Water Resour. Prot.*, 35(1): 27-34, 2019a.
- 585 Chen, H., Yong, B., Gourly, J. J., Liu, J., Ren, L., Wang, W., Hong, Y., and Zhang, J.: Impact of the Crucial Geographical and Climatic Factors on the Input Source Errors of GPM-based Global Satellite Precipitation Estimates, *J. Hydrol.*, 575, 1-16, <https://doi.org/10.1016/j.jhydrol.2019.05.020>, 2019b.



- Chen, H., Yong, B., Shen, Y., Liu, J., Hong, Y., and Zhang, J.: Comparison analysis of
590 six purely satellite-derived global precipitation estimates, *J. Hydrol.*, 581, 124376,
<https://doi.org/10.1016/j.jhydrol.2019.124376>, 2020.
- Chen, M., Shi, W., Xie, P., Silva, V. B., Kousky, V. E., Wayne Higgins, R., and Janowiak,
J. E.: Assessing objective techniques for gauge - based analyses of global daily
precipitation, *J. Geophys. Res.-Atmos.*, 113(D4), 2008.
- 595 Chen, S., Hong, Y., Cao, Q., Gourley, J. J., Kirstetter, P. E., Yong, B., Tian, Y., Zhang,
Z. X., Shen, Y., Hu, J. J., and Hardy, J.: Similarity and difference of the two successive
V6 and V7 TRMM multisatellite precipitation analysis performance over China, *J.*
Geophys. Res.-Atmos., 118(23), 2013.
- Choubin, B., Khalighisigaroodi, S., Mishra, A. K., Goodarzi, M., Shamshirband, S.,
600 Ghaljaee, E., and Zhang, F.: A novel bias correction framework of TMPA 3B42 daily
precipitation data using similarity matrix/homogeneous conditions, *Sci. Total Environ.*,
694, 133680, <https://doi.org/10.1016/j.scitotenv.2019.133680>, 2019.
- Gebregiorgis, A. S., Kirstetter, P.-E., Hong, Y. E., Gourley, J. J., Huffman, G. J.,
Petersen, W. A., Xue, X., and Schwaller, M. R.: To what extent is the day 1 GPM
605 IMERG satellite precipitation estimate improved as compared to TRMM TMPA-RT?,
J. Geophys. Res.-Atmos., 123, 1694-1707, 2018.
- Guo, H., Bao, A., Ndayisaba, F., Liu, T., Kurban, A., and De Maeyer, P.: Systematical
Evaluation of Satellite Precipitation Estimates Over Central Asia Using an Improved
Error-Component Procedure, *J. Geophys. Res.-Atmos.*, 122, 10906-10927,
610 <https://doi.org/10.1002/2017JD026877>, 2017.



- Hashemi, H., Nordin, M., Lakshmi, V., Huffman, G. J., and Knight, R.: Bias Correction of Long-Term Satellite Monthly Precipitation Product (TRMM 3B43) over the Conterminous United States, *J. Hydrometeorol.*, 18, 2491-2509, DOI: 10.1175/JHM-D-17-0025.1, 2017.
- 615 Hong, Y., Hsu, K. L., Sorooshian, S., and Gao, X.: Precipitation estimation from remotely sensed imagery using an artificial neural network cloud classification system, *J. Appl. Meteorol.*, 43, 1834–1853, 2004.
- Hou, A. Y., Kakar, R. K., Neeck, S., Azarbarzin, A. A., Kummerow, C. D., Kojima, M., Oki, R., Nakamura, K., and Lguchi, T.: The global precipitation measurement
620 mission, *Bull. Am. Meteorol. Soc.*, 95(5), 701-722, 2014.
- Huffman, G. J., Bolvin, D. T., Nelkin, E. J., and Tan, J.: Integrated Multi-satellitE Retrievals for GPM (IMERG) Technical Documentation, NASA/GSFC, pp. 1, 2019.
- Kidd, C., and Levizzani, V.: Status of satellite precipitation retrievals, *Hydrol. Earth Syst. Sci.*, 15, 1109-1116, <https://doi.org/10.5194/hess-15-1109-2011>, 2011a.
- 625 Kidd, C., Becker, A., Huffman, G. J., Muller, C. L., Joe, P., Skofronick-Jackson, G., and Kirschbaum, D. B.: So, how much of the Earth’s surface is covered by rain gauges?, *Bull. Am. Meteorol. Soc.*, 98(1), 69-78, 2017.
- Kidd, C., and Huffman, G. J.: Global precipitation measurement, *Meteorol. Appl.*, 18(3), 334-353, 2011b.
- 630 Kirstetter, P. E., Hong, Y., Gourley, J. J., Schwaller, M., Petersen, W., and Zhang, J.: Comparison of TRMM 2A25 products, version 6 and version 7, with NOAA/NSSL ground radar-based National Mosaic QPE, *J. Hydrometeorol.*, 14(2), 661-669, 2013.



- Kubota, T., Shige, S., Hashizume, H., Aonashi, K., Takahashi, N., Seto, S., Hirose, M.,
Takayabu, Y. N., Ushio, T., Nakagawa, K., Iwanami, K., Kachi, M., and Okamoto, K.:
635 Global precipitation map using satellite-borne microwave radiometers by the gsmap
project: production and validation, *IEEE Trans. Geosci. Remote Sens.*, 45(7), 2259-
2275, 2007.
- Le, H. M., Sutton, J. R., Du Bui, D., Bolten, J. D., and Lakshmi, V.: Comparison and
Bias Correction of TMPA Precipitation Products over the Lower Part of Red–Thai Binh
640 River Basin of Vietnam, *Remote Sens.*, 10, 1582, doi:10.3390/rs10101582, 2018.
- Liu, Z.: Comparison of ntegrated Multi-satellite Retrievals for GPM (IMERG) and
TRMM Multi-satellite Precipitation Analysis (TMPA) monthly precipitation products:
initial results, *J. Hydrometeorol.*, 17(3), 777-790, 2016.
- Maggioni, V., Meyers, P. C., and Robinson, M. D.: A review of merged high-resolution
645 satellite precipitation product accuracy during the Tropical Rainfall Measuring Mission
(TRMM) era, *J. Hydrometeorol.*, 17(4), 1101-1117, 2016a.
- Maggioni, V., Sapiano, M. R., and Adler, R. F.: Estimating Uncertainties in High-
Resolution Satellite Precipitation Products: Systematic or Random Error?, *J.*
Hydrometeorol., 17(4), 1119-1129, 2016b.
- 650 Prakash, S., Mitra, A. K., AghaKouchak, A., Liu, Z., Norouzi, H., and Pai, D. S.: A
preliminary assessment of GPM-based multi-satellite precipitation estimates over a
monsoon dominated region, *J. Hydrol.*, 556, 865-876, 2018.
- Shen, G., Chen, N., Wang, W., and Chen, Z.: WHU-SGCC: a novel approach for
blending daily satellite (CHIRP) and precipitation observations over the Jinsha River



- 655 basin, *Earth Syst. Sci. Data*, 11(4), 1711-1744, 2019.
- Shen, Y., and Xiong, A.: Validation and comparison of a new gauge-based precipitation analysis over mainland China, *Int. J. Climatol.*, 36, 252–265, 2016.
- Sorooshian, S., Hsu, K. L., Gao, X., Gupta, H. V., Imam, B., and Braithwaite, D.: Evaluation of PERSIANN system satellite-based estimates of tropical rainfall, *Bull. Am. Meteorol. Soc.*, 81(9), 2035-2046, 2000.
- 660 Su, J., Lü, H., Zhu, Y., Wang, X., and Wei, G.: Component analysis of errors in four GPM-based precipitation estimations over Mainland China, *Remote Sens.*, 10(9), 1420, 2018.
- Takido, K., Valeriano, O. C. S., Ryo, M., Tanuma, K., Ushio, T., and Kubota, T.: 665 Spatiotemporal evaluation of the gauge-adjusted global satellite mapping of precipitation at the basin scale, *J. Meteorol. Soc. Jpn.*, 94(2), 185-195, 2016.
- Tan, J., Petersen, W. A., Kirstetter, P. E., and Tian, Y.: Performance of IMERG as a function of spatiotemporal scale, *J. Hydrometeorol.*, 18(2), 307-319, 2017.
- Tapiador, F. J., Turk, F. J., Petersen, W., Hou, A.Y., García-Ortega, E., Machado, L. A. 670 T., Angelis, C. F., Salio, P., Kidd, C., Huffman, G. J., and de Castro, M.: Global precipitation measurement: methods, datasets and applications, *Atmos. Res.*, 105, 70–97, <https://doi.org/10.1016/j.atmosres.2011.10.021>, 2012.
- Tian, Y., and Peters-Lidard, C. D.: A global map of uncertainties in satellite-based precipitation measurements, *Geophys. Res. Lett.*, 37, L24407, 675 doi:10.1029/2010GL046008, 2010a.
- Tian, Y., Peterslidard, C. D., and Eylander, J. B.: Real-Time Bias Reduction for



- Satellite-Based Precipitation Estimates, *J. Hydrometeorol.*, 11(6), 1275-1285, 2010b.
- Tian, Y., Peters-Lidard, C. D., Eylander, J. B., Joyce, R. J., Huffman, G. J., Adler, R. F.,
Hsu, K. L., Turk, F. J., Garcia, M., and Zeng, J.: Component analysis of errors in
680 satellite-based precipitation estimates, *J. Geophys. Res.-Atmos.* 114(D24), 2009.
- Ushio, T., Sasashige, K., Kubota, T., Shige, S., Okamoto, K. I., Aonashi, K., Inoue, T.,
Takahashi, N., Iguchi, T., Kachi, M., Oki, R., Morimoto, T., and Kawasaki, Z. I.: A
Kalman filter approach to the Global Satellite Mapping of Precipitation (GSMaP) from
combined passive microwave and infrared radiometric data, *J. Meteorol. Soc. Jpn. Ser.*
685 *II*, 87, 137-151, 2009.
- Willmott, J.: On the validation of model, *Phys. Geogr.*, 2, 184–194, 1981.
- Xie, P., Chen, M., Yang, S., Yatagai, A., Hayasaka, T., Fukushima, Y., and Liu, C.: A
gauge-based analysis of daily precipitation over East Asia, *J. Hydrometeorol.*, 8(3),
607-626, 2007.
- 690 Xu, R., Tian, F., Yang, L., Hu, H., Lu, H., and Hou, A.: Ground validation of GPM
IMERG and TRMM 3B42V7 rainfall products over southern Tibetan Plateau based on
a high - density rain gauge network, *J. Geophys. Res.-Atmos.*, 122(2), 910-924,
doi:10.1002/2016JD025418, 2017.
- Xu, S., Shen, Y., and Du, Z.: Tracing the source of the errors in hourly IMERG using a
695 decomposition evaluation scheme, *Atmosphere*, 7(12), 161,
doi:10.3390/atmos7120161, 2016.
- Yamamoto, M. K., and Shige, S.: Implementation of an orographic/nonorographic
rainfall classification scheme in the GSMaP algorithm for microwave



radiometers, *Atmos. Res.*, 163, 36-47, 2015.

700 Yong, B., Chen, B., Tian, Y., Yu, Z., and Hong, Y.: Error-component analysis of TRMM-
based multi-satellite precipitation estimates over mainland China, *Remote Sens.*, 8(5),
440, 2016.

Yong, B., Liu, D., Gourley, J. J., Tian, Y., Huffman, G. J., Ren, L., and Hong, Y.: Global
view of real-time TRMM multisatellite precipitation analysis: Implications for its
705 successor global precipitation measurement mission, *Bull. Am. Meteorol. Soc.*, 96(2),
283-296, 2015.

Yong, B., Ren, L., Hong, Y., Gourley, J. J., Tian, Y., Huffman, G. J., Chen X., Wang W.
G., and Wen, Y. X.: First evaluation of the climatological calibration algorithm in the
real - time TMPA precipitation estimates over two basins at high and low
710 latitudes, *Water Resour. Res.*, 49(5), 2461-2472, 2013.

Yong, B., Ren, L., Hong, Y., Wang, J. H., Gourley, J. J., Jiang, S., Chen, X., and Wang,
W.: Hydrologic evaluation of Multisatellite Precipitation Analysis standard
precipitation products in basins beyond its inclined latitude band: A case study in
Laohahe basin, China, *Water Resour. Res.*, 46, W07542, doi :10.1029/2009WR008965,
715 2010.



Figure and Table Captions

Fig. 1. (a) Global map of topography; (b) mean annual precipitation of the global land from 1891 to 2018 (128 years); (c) global land is divided into four climate areas (i.e., humid, semi-humid, semi-arid, arid); (d) the spatial maps of rain gauges used in Climate Precipitation Center unified (CPCU) data and China Gauge-based Daily Precipitation Analysis (CGDPA) data.

Fig. 2. Global maps of the total bias and its three independent components for the three satellite-only precipitation global precipitation estimates (i.e., IMERG-Late, GSMaP-MVK, and PERSIANN-CCS) at a 0.5° spatial and daily temporal resolution in the MAM season across global land for the period from 2015 to 2019 (5 years): (a-d) IMERG-Late, (e-h) GSMaP-MVK, (i-l) PERSIANN-CCS.

Fig. 3. As in Fig. 2 for JJA season.

Fig. 4. As in Fig. 2 for SON season.

Fig. 5. As in Fig. 2 for DJF season.

Fig. 6. Global maps of the systematic errors for the three satellite-only global precipitation estimates (i.e., IMERG-Late, GSMaP-MVK, and PERSIANN-CCS) at a 0.5° spatial and daily temporal resolution in four seasons (i.e., MAM, JJA, SON, and DJF) over global land for the period from 2015 to 2019 (5 years): (a-d) IMERG-Late, (e-h) GSMaP-MVK, (i-l) PERSIANN-CCS.

Fig. 7. The four bias scores (i.e., total bias, hit bias, miss bias, and false bias) for the five satellite-only global precipitation estimates (i.e., IMERG-Late, IMERG-Early,



GSMaP-MVK, GSMaP-NRT, and PERSIANN-CCS) at a 0.5° spatial and daily temporal resolution under different rainfall intensities. Note that the precipitation intensity categories are from references.

Fig. 8. As in Fig. 7 for systematic error.

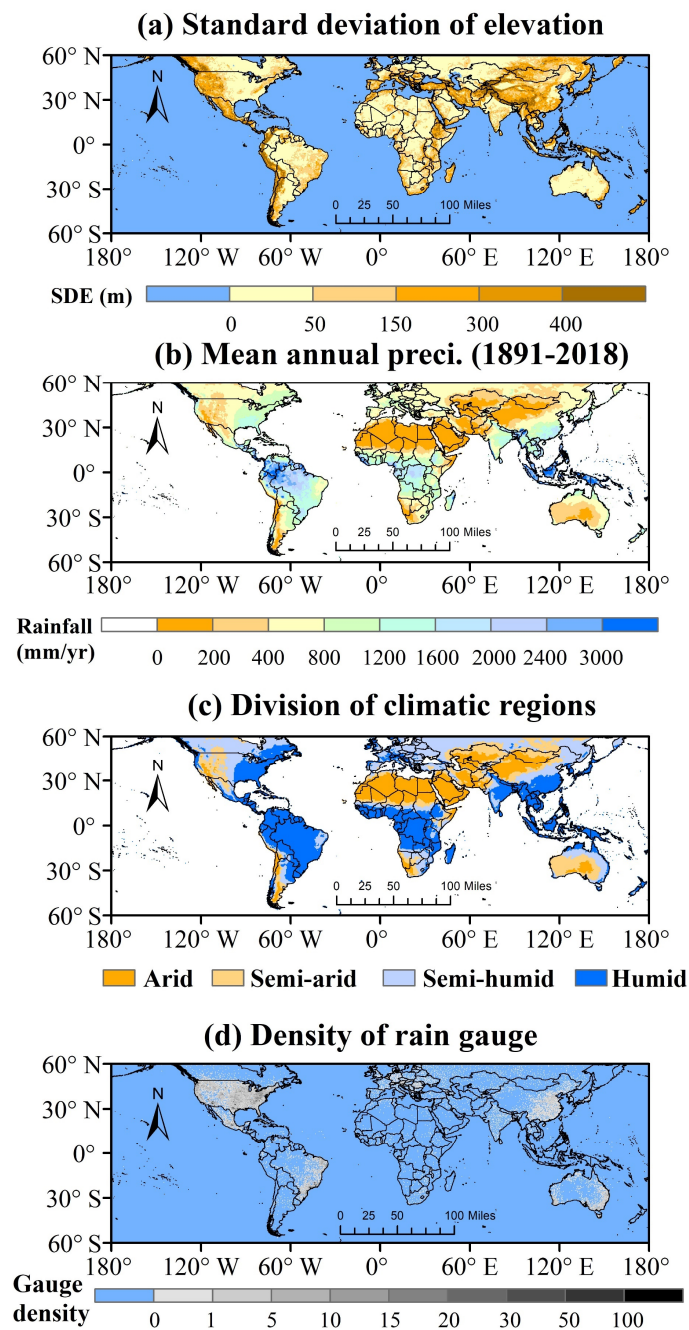
Fig. 9. The four bias scores (i.e., total bias, hit bias, miss bias, and false bias) for the five satellite-only global precipitation estimates (i.e., IMERG-Late, IMERG-Early, GSMaP-MVK, GSMaP-NRT, and PERSIANN-CCS) under different terrains. Note that the analysis executed at a 0.1° spatial and hourly temporal resolution in the humid regions of mainland China over JJA (summer) season for the period from 2015 to 2019 (5 years).

Fig. 10. (a) Systematic errors for the five satellite-only global precipitation estimates (i.e., IMERG-Late, IMERG-Early, GSMaP-MVK, GSMaP-NRT, and PERSIANN-CCS) under different topographies; (b) the variations of normalized error component (NEC) for the five satellite-only global precipitation estimates with increasing terrain complexity. Note that the analysis executed at a 0.1° spatial and hourly temporal resolution in the humid regions of mainland China over JJA (summer) season for the period from 2015 to 2019 (5 years).

Table 1 The information about five satellite-only global precipitation estimates used in this study.



Figures



760 **Fig. 1.** (a) Global map of topography; (b) mean annual precipitation of the global land



from 1891 to 2018 (128 years); (c) global land is divided into four climate areas (i.e., humid, semi-humid, semi-arid, arid); (d) the spatial maps of rain gauges used in Climate Precipitation Center unified (CPCU) data and China Gauge-based Daily Precipitation Analysis (CGDPA) data.

765

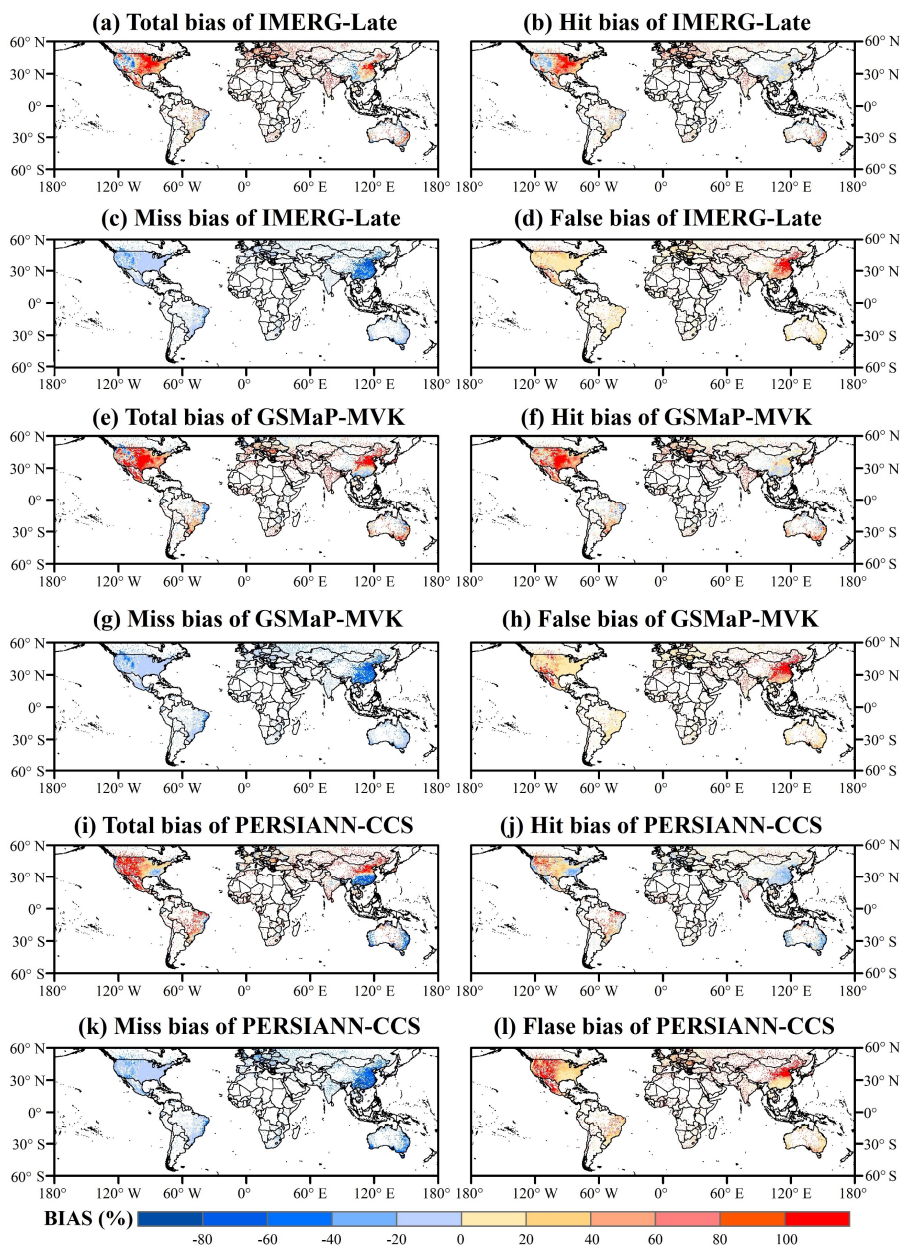


Fig. 2. Global maps of the total bias and its three independent components for the three satellite-only precipitation global precipitation estimates (i.e., IMERG-Late, GSMaP-MVK, and PERSIANN-CCS) at a 0.5° spatial and daily temporal resolution in the



770 MAM season across global land for the period from 2015 to 2019 (5 years): (a-d)
IMERG-Late, (e-h) GSMaP-MVK, (i-l) PERSIANN-CCS.

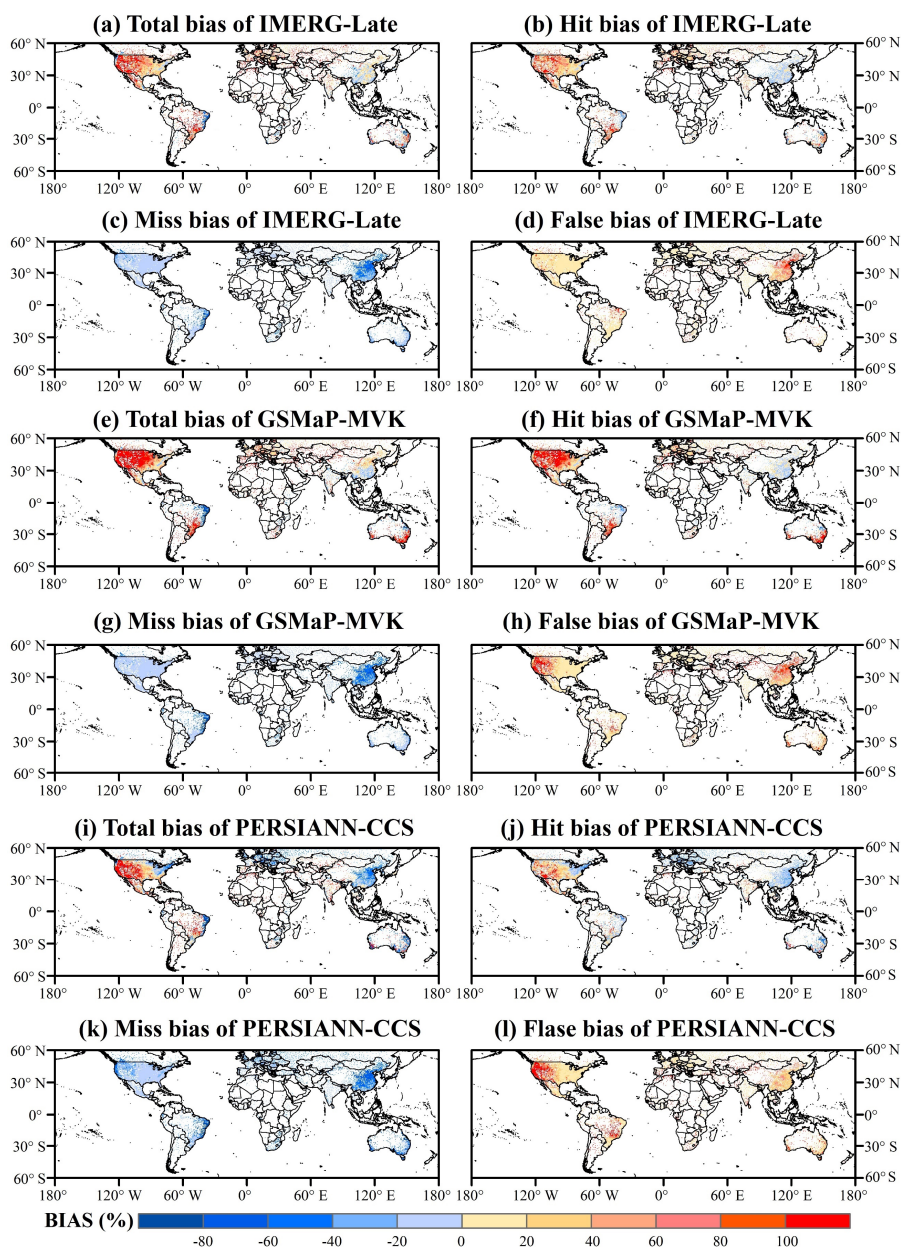


Fig. 3. As in Fig. 2 for JJA season.

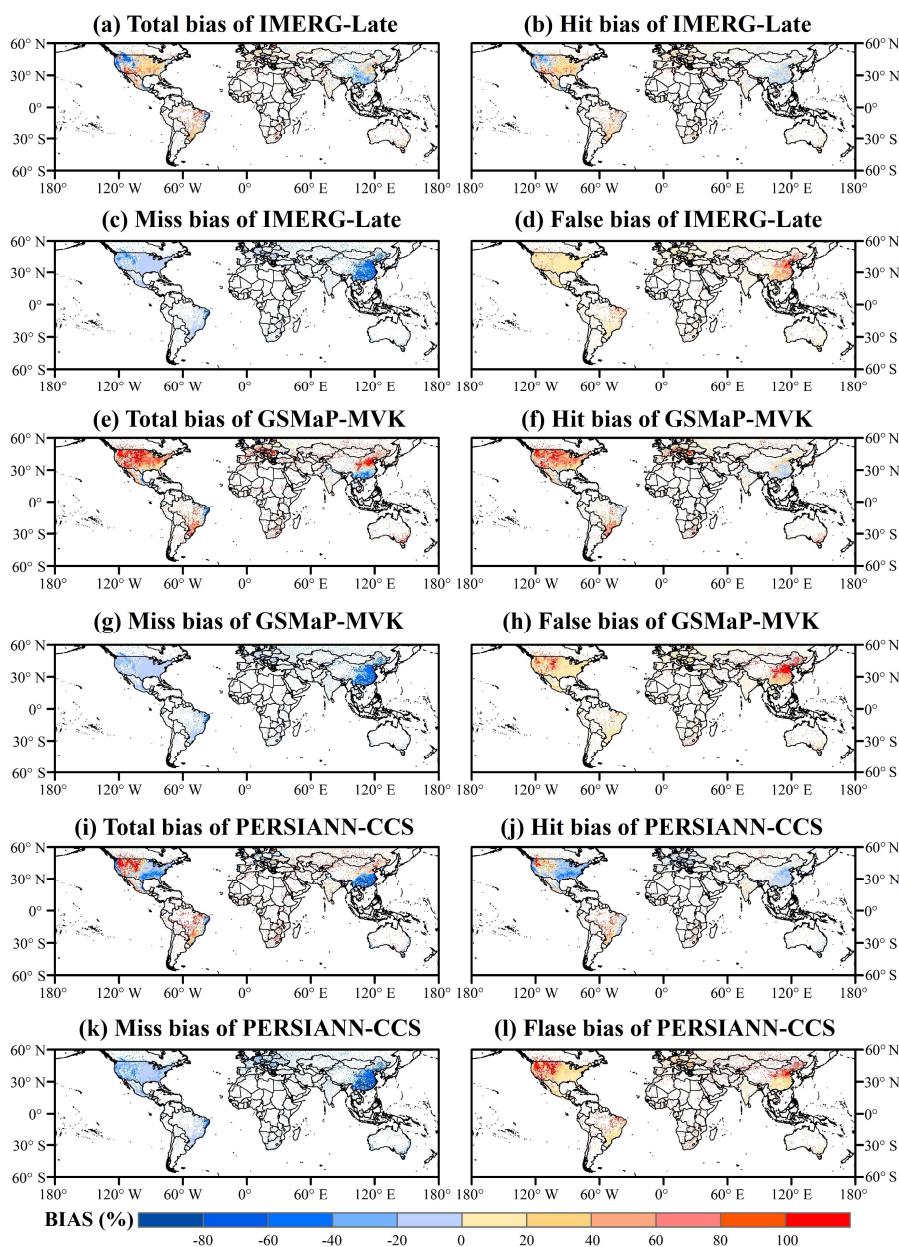
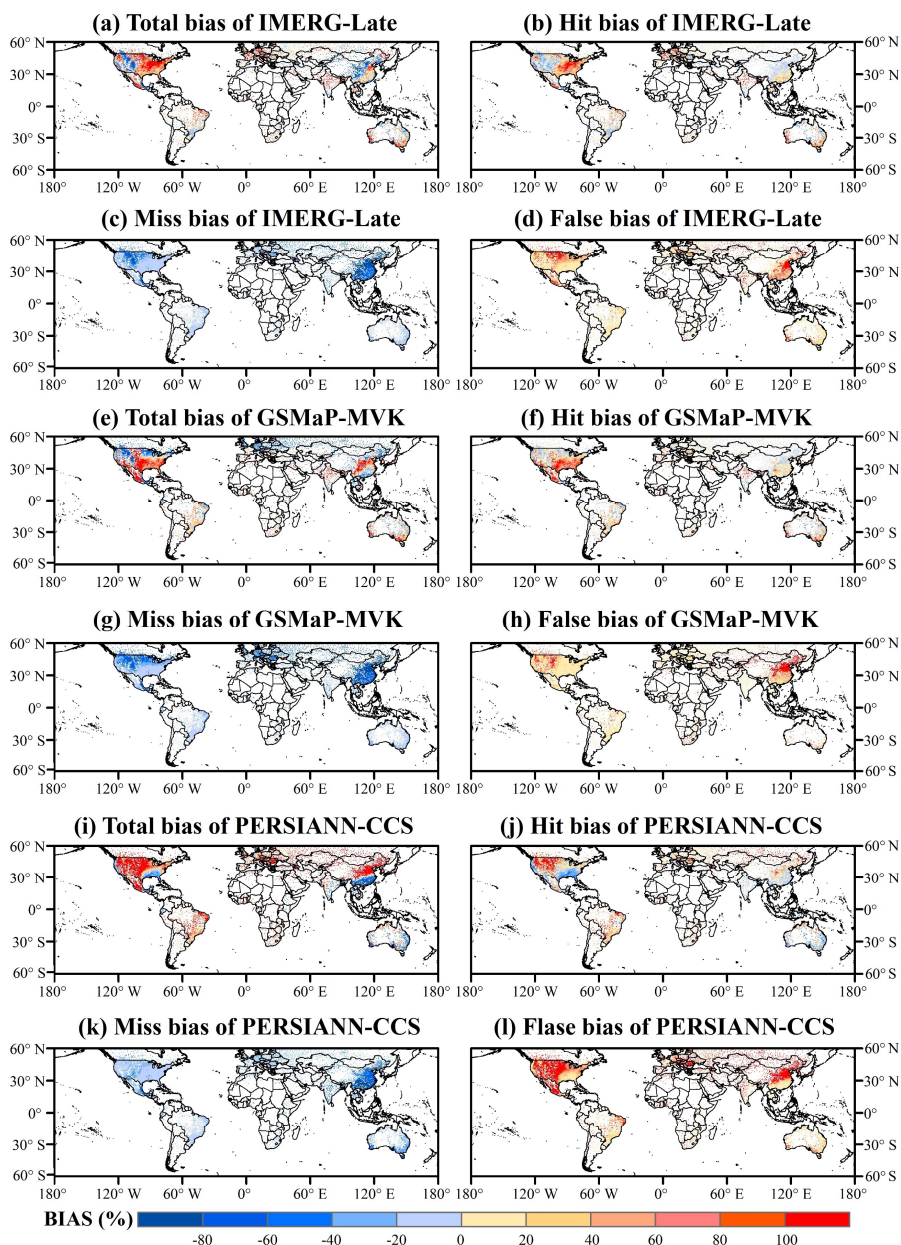


Fig. 4. As in Fig. 2 for SON season.



780 **Fig. 5.** As in Fig. 2 for DJF season.

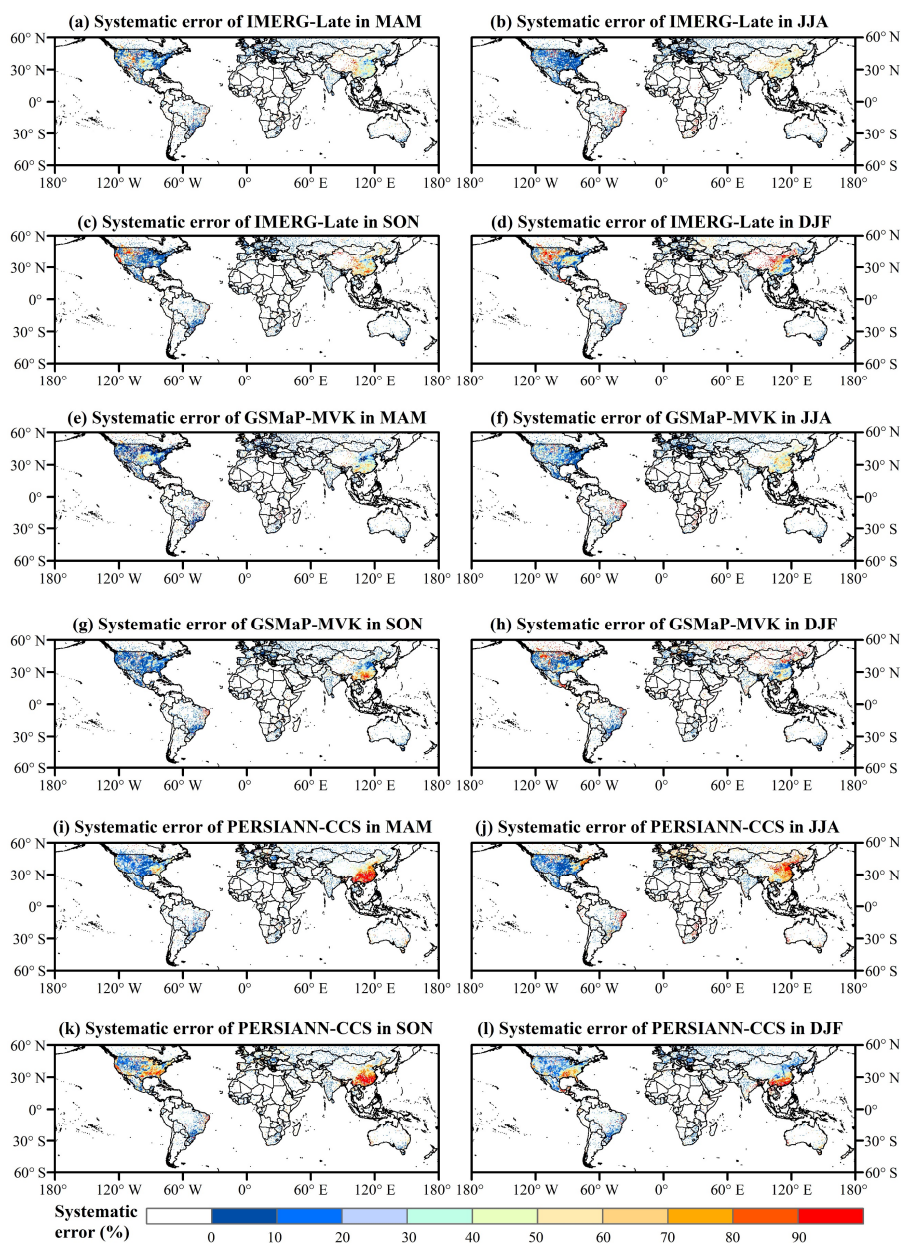
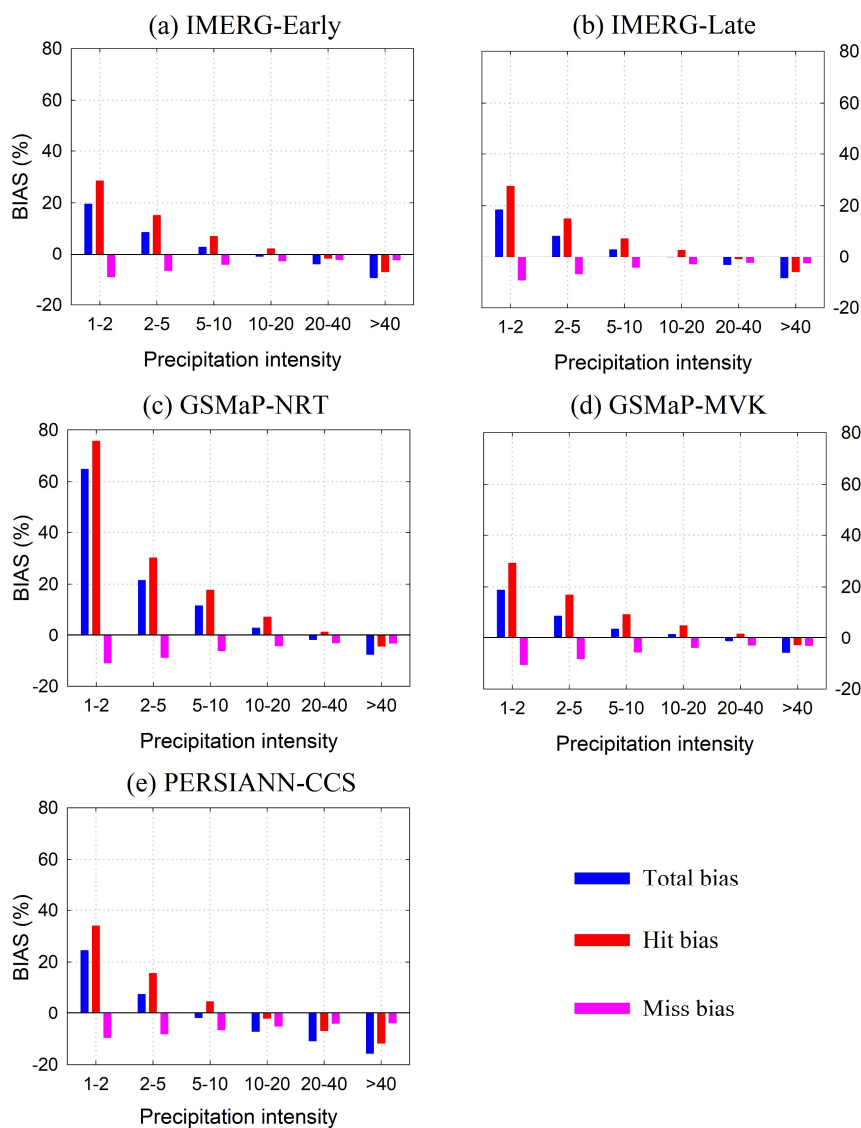


Fig. 6. Global maps of the systematic errors for the three satellite-only global precipitation estimates (i.e., IMERG-Late, GSMaP-MVK, and PERSIANN-CCS) at a

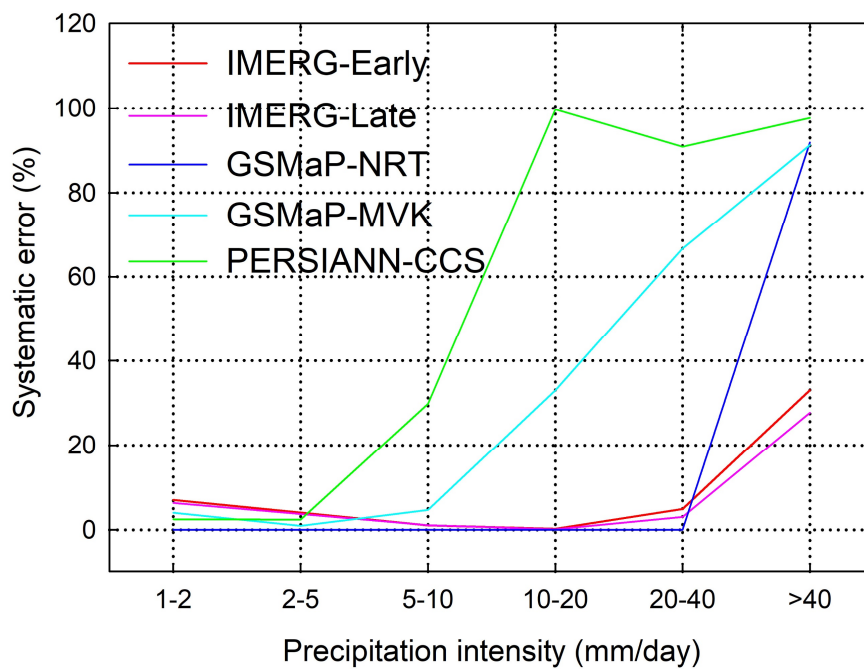
785 0.5° spatial and daily temporal resolution in four seasons (i.e., MAM, JJA, SON, and



DJF) over global land for the period from 2015 to 2019 (5 years): (a-d) IMERG-Late,
(e-h) GSMaP-MVK, (i-l) PERSIANN-CCS.



790 **Fig. 7.** The four bias scores (i.e., total bias, hit bias, miss bias, and false bias) for the
 five satellite-only global precipitation estimates (i.e., IMERG-Late, IMERG-Early,
 GSMaP-MVK, GSMaP-NRT, and PERSIANN-CCS) at a 0.5° spatial and daily
 temporal resolution under different rainfall intensities. Note that the precipitation
 intensity categories are from references.



795

Fig. 8. As in Fig. 7 for systematic error.

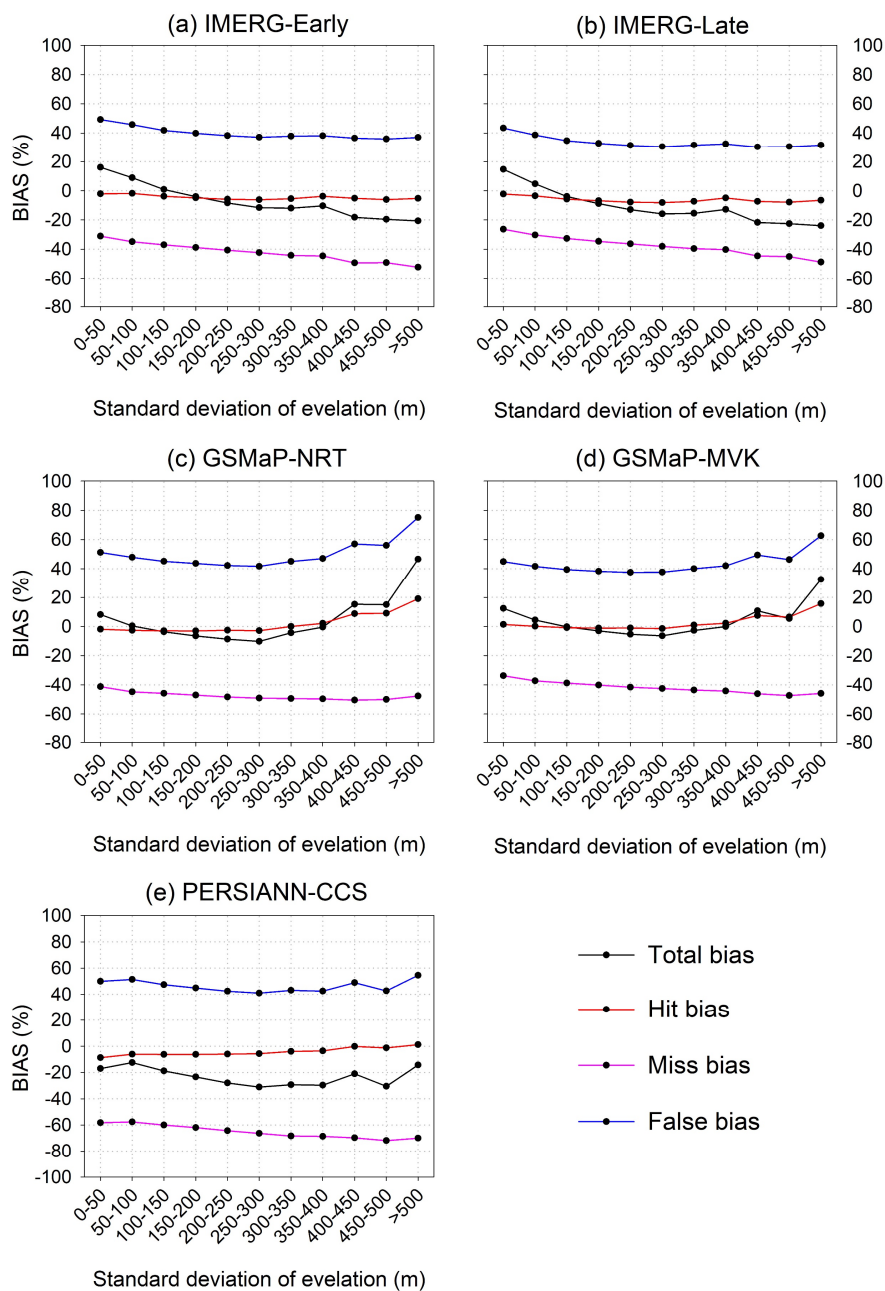


Fig. 9. The four bias scores (i.e., total bias, hit bias, miss bias, and false bias) for the 800 five satellite-only global precipitation estimates (i.e., IMERG-Late, IMERG-Early,



GSMaP-MVK, GSMaP-NRT, and PERSIANN-CCS) under different terrains. Note that the analysis executed at a 0.1° spatial and hourly temporal resolution in the humid regions of mainland China over JJA (summer) season for the period from 2015 to 2019 (5 years).

805

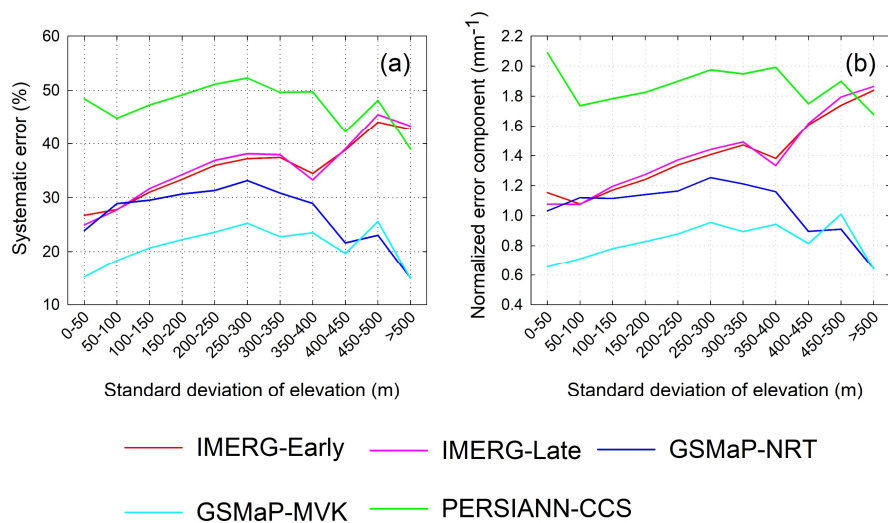


Fig. 10. (a) Systematic errors for the five satellite-only global precipitation estimates (i.e., IMERG-Late, IMERG-Early, GSMaP-MVK, GSMaP-NRT, and PERSIANN-CCS) under different topographies; (b) the variations of normalized error component
 810 (NEC) for the five satellite-only global precipitation estimates with increasing terrain complexity. Note that the analysis executed at a 0.1° spatial and hourly temporal resolution in the humid regions of mainland China over JJA (summer) season for the period from 2015 to 2019 (5 years).



814 **Tables**

815 **Table 1** The information about five satellite-only global precipitation estimates used in
 816 this study.

Product	Full name of product	Data source	Resolution	Reference (s)
IMERG-Late	Integrated Multi-satellitE Retrievals for GPM Late run V06B	PMW, IR	0.1°/0.5h	Huffman et al. (2019)
IMERG-Early	Integrated Multi-satellitE Retrievals for GPM Early run V06B	PMW, IR	0.1°/0.5h	Huffman et al. (2019)
GSMaP-MVK	Global Satellite Mapping of Precipitation Microwave-IR Combined Product V7	PMW, IR	0.1°/1h	Ushio et al. (2009)
GSMaP-NRT	Global Satellite Mapping of Precipitation in Near-Real-Time V6/V7	PMW, IR	0.1°/1h	Kubota et al. (2007)
PERSIANN-CCS	Precipitation Estimation from Remotely Sensed Information using Neural Networks Cloud Classification	IR	0.04°/1h	Sorooshian et al. (2000); Hong et al. (2004)